

Nanoprobes for Biomedical Imaging with Tunable Near-Infrared Optical Properties Obtained via Green Synthesis

Riccardo Marin,^{*} Antonio Benayas, Nuria García-Carillo, José Lifante, Jingke Yao, Diego Mendez-Gonzalez, Francisco Sanz-Rodríguez, Jorge Rubio-Retama, Lucas V. Besteiro, and Daniel Jaque^{*}

Ideally, any material used should be nontoxic and produced with safe, inexpensive, and energy-effective processes. In the case of optically active nanoparticles, this is often not the case, as they are frequently composed of hazardous heavy metals and/or produced with methods far from being environmentally friendly. Herein, the preparation of Ag₂S-based nanoparticles via a simple green synthesis route is explored. Aqueous extracts of roasted coffee are used as sources of coordinating molecules. Optimization of the reaction conditions yields dimeric Ag–Ag₂S nanoparticles, whose near-infrared photoluminescence can be switched on via H₂O₂-mediated oxidation. This oxidation transforms suitable photoacoustic contrast agents into fluorescence imaging probes. Theoretical calculations further clarify the role of metallic silver in determining the optical properties of Ag₂S. Overall, it is demonstrated that nanomaterials with tangible applicative potential can be prepared via cost- and energy-effective synthesis strategies that entail benign, renewable chemicals.

environmental awareness has been increasing at every level of the society and the industry, with the implementation of more sustainable solutions. Nanotechnology is no exception to this trend. The availability of heavy metal-free nanomaterials having performance on par with less environmentally friendly ones and the development of greener synthesis methods are urgent matters.^[2] Silver^[3,4] and gold^[5,6] nanoparticles can be easily prepared with energy-inexpensive approaches, using renewable sources and chemical species that pose little-to-no threat to the environment. Instead, the preparation of metal chalcogenides nanoparticles via green methods is less straightforward.

Belonging to this family of nanomaterials, Ag₂S nanoparticles are particularly appealing species due to their optical activity (absorption and emission) in the near-infrared (NIR) region.^[7]


Their benign chemical composition and demonstrated biocompatibility make them amenable to a broad range of applications, including nanomedicine.^[8] Indeed, they have been proposed as contrast agents for photoacoustic (PAI) and fluorescence imaging (FI).^[8–11] Well-established synthesis methods for the preparation of Ag₂S nanoparticles rely on organic high-boiling

1. Introduction

With its Goal 12, the United Nations #Envision2030 agenda targets the achievement of “environmentally sound management of chemicals and all wastes throughout their life cycle” and “sustainable management and efficient use of natural resources”.^[1] Generally speaking, over the past years,

R. Marin, A. Benayas, J. Yao, D. Mendez-Gonzalez, D. Jaque
Nanomaterials for Bioimaging Group (nanoBIG)
Departamento de Física de Materiales
Facultad de Ciencias
Universidad Autónoma de Madrid
C/ Francisco Tomás y Valiente 7, Madrid 28049, Spain
E-mail: riccardo.marin@uam.es; daniel.jaque@uam.es

A. Benayas, J. Lifante, D. Mendez-Gonzalez, F. Sanz-Rodríguez,
J. Rubio-Retama, D. Jaque
Nanomaterials for Bioimaging Group (nanoBIG)
Instituto Ramón y Cajal de Investigación Sanitaria
Hospital Ramón y Cajal
Ctra. De Colmenar Viejo, Km. 9100, Madrid 28034, Spain

 The ORCID identification number(s) for the author(s) of this article can be found under <https://doi.org/10.1002/adpr.202100260>.

© 2021 The Authors. Advanced Photonics Research published by Wiley-VCH GmbH. This is an open access article under the terms of the Creative Commons Attribution License, which permits use, distribution and reproduction in any medium, provided the original work is properly cited.

DOI: 10.1002/adpr.202100260

N. García-Carillo
Laboratory Animal Service
University of Murcia
Murcia 30100, Spain

F. Sanz-Rodríguez
Nanomaterials for Bioimaging Group (nanoBIG)
Departamento de Biología
Facultad de Ciencias
Universidad Autónoma de Madrid
C/ Darwin 2, Madrid 28049, Spain

J. Rubio-Retama
Department of Chemistry in Pharmaceutical Sciences
Pharmacy Faculty
Complutense University of Madrid
Plaza de Ramón y Cajal S/N, Madrid 28040, Spain

L. V. Besteiro
CINBIO
Universidade de Vigo
Vigo 36310, Spain

solvents/ligands (e.g., octadecene, oleylamine, dodecanethiol), are energy intensive (i.e., use high reaction temperatures), and require surface modification to impart water dispersibility.^[12,13] Recently, a widely applicable green method for the synthesis of hydrophobic metal sulfide nanoparticles was developed by Yuan et al., which uses an ionic liquid prepared by reacting H₂S and oleylamine.^[14] Despite the reusability of the ionic liquid, the use of H₂S poses safety concerns. In addition, mesitylene (a benzene derivative) has to be used as a thinning solvent to conduct reactions at room temperature. In contrast, aqueous methods afford Ag₂S nanoparticles that are readily dispersible in water, while allaying concerns over the handling of dangerous/toxic solvents. However, these methods generally entail the use of mercaptoalkyl acids—which are toxic and corrosive—and/or heating above room temperature.^[15,16] When plant extracts are used, control over the precursors reactivity is difficult to achieve and thus the Ag₂S nanoparticles have broad size distribution or highly irregular morphology.^[17,18] Bacteria-mediated syntheses have also been developed, but they usually have low yields (<50–60%) and are labor intensive.^[19] Alternative, versatile, and efficient green methods to produce Ag₂S nanoparticles are therefore necessary.

In this work, we showcase a novel green synthesis approach for the preparation of Ag₂S-based nanoparticles to be used in PAI and FI. The green nature of the synthesis method follows from its safety, cost- and energy-effectiveness, and the use of store-bought roasted coffee extract as a renewable source of growth-directing molecules. Among the range of nanoparticles that can be synthesized with the developed method, nanometric Ag–Ag₂S dimers showed particularly strong light absorption properties and lack of photoluminescence (PL), making them ideal PAI contrast agents. The PL of these species could be switched on via deliberate oxidation of the Ag moiety, thus making them viable FI contrast agents. Insight into the role played by silver in determining the optical properties of these nanomaterials was obtained both from experimental analysis and from

theoretical simulations. These results are a step in the direction of a more environmentally friendly approach for the preparation of nanoparticles as functional materials for real-life applications.

2. Results and Discussion

2.1. Green Synthesis of Ag₂S-Based Nanoparticles

The developed green synthesis method relies on the presence of molecules acting as reducing agents and stabilizers/capping agents in the roasted coffee extract. These are mainly species bearing carboxylic and hydroxyl groups, such as chlorogenic acids (e.g., 5-caffeoylquinic acid), trigonelline, niacin, sucrose, and arabinogalactans (Figure 1).^[20] The said water-soluble molecules were extracted from roasted coffee powder via a “cold brew”-like extraction method. Brewing at lower temperatures is known to yield a coffee extract with higher pH compared with “hot brews”, due to slightly less-efficient acid extraction.^[21] As we were interested particularly in these molecules for our synthetic purposes, cold extraction seems less suitable than hot extraction. However, the use of water at room temperature minimizes the extraction of more hydrophobic substances, which would ultimately be detrimental to the water dispersibility of the produced nanoparticles. The “cold brew” approach was preferred also in the spirit of a greener synthesis approach, due to its less energy-expensive nature compared with high-temperature extraction. For the same reason, we also decided to conduct synthesis of the nanoparticles at room temperature.

In the proposed synthesis method, the order of addition of the precursors to the reaction mixture and control over the pH are the two key aspects. Indeed, depending on these two parameters, different nanoparticles could be obtained: Ag or Ag₂S nanoparticles and Ag–Ag₂S dimers (Figure 1, 2). The versatility of this synthesis approach follows from the reducing capability of the coffee extract versus Ag⁺ ions. In a typical synthesis, a diluted solution of coffee extract is prepared, whose pH is ≈5.5. If

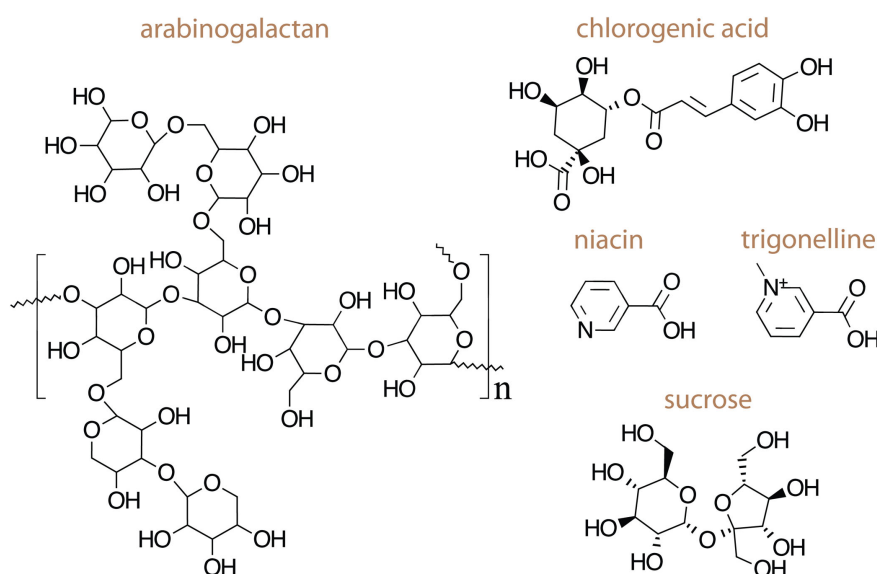


Figure 1. Molecular structure of some of the molecules in roasted coffee extract that can show coordinating capabilities toward metallic ions in solution.

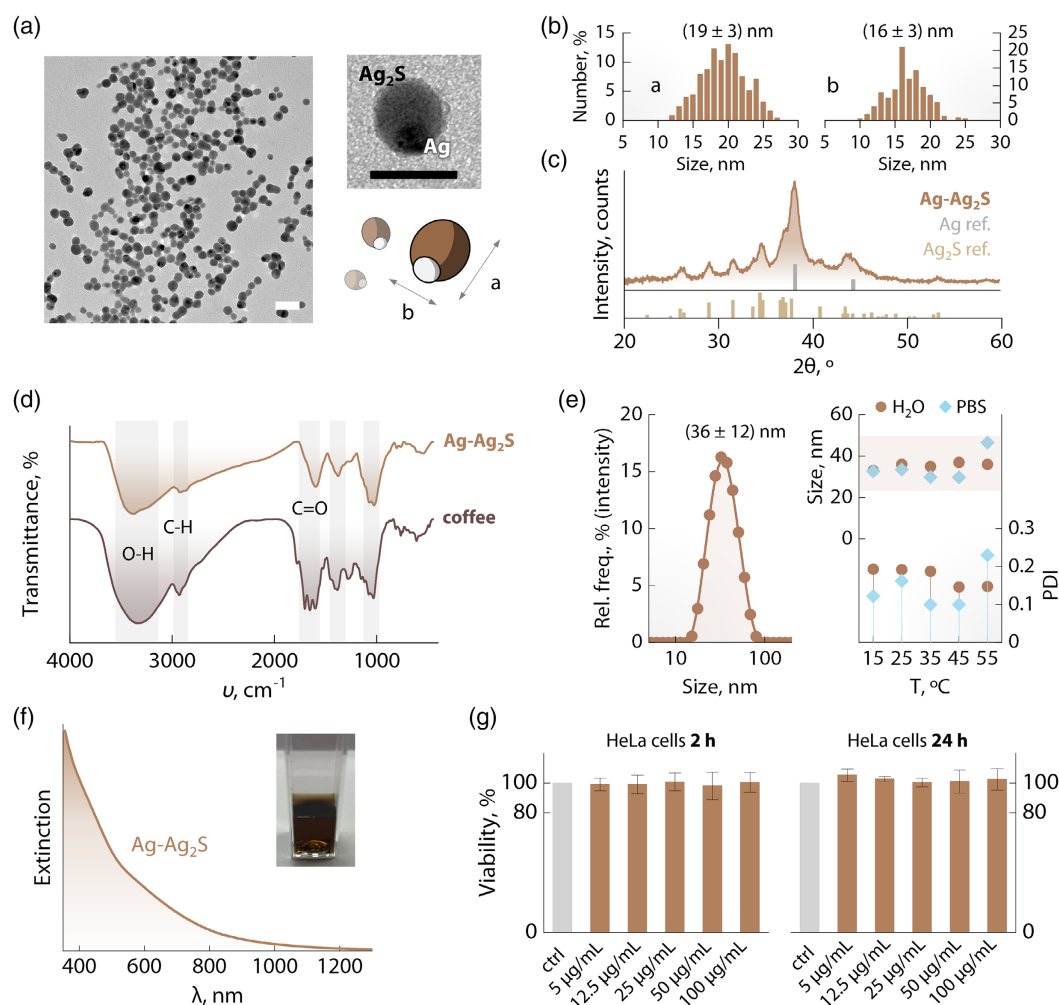


Figure 2. Characterization of Ag-Ag₂S dimers. a) Representative TEM image of Ag-Ag₂S dimers (scale bar = 50 nm), along with a zoom-in on an isolated dimer where the Ag₂S and Ag moieties are discernible, and an artistic representation of typical dimers observed. The major (a) and minor (b) axes are also indicated. b) Size distribution for the major and minor axes obtained from the measurement of 200 dimers. Mean value and standard deviations were obtained as the first moment and the square root of the second moment of the distributions, respectively. c) XRPD pattern of the Ag-Ag₂S dimers (solid line) and the reference patterns of Ag (PDF #00-004-0783, gray bars) and Ag₂S (PDF #00-014-0072, golden bars). d) FTIR spectra of Ag-Ag₂S and dried coffee extract. Shaded rectangles are drawn in correspondence to the wavenumber ranges where comparable signals are observed for dried coffee extract and Ag-Ag₂S dimers. The regions where the vibrations of O-H, C-H, and C=O groups fall are labeled. e) Results of DLS measurements conducted on a Ag-Ag₂S dimer dispersion in phosphate buffer saline (PBS 1×) at room temperature (left) and the trend of the average hydrodynamic diameter and polydispersity index (PDI) in water (light blue diamonds) and PBS 1× (brown circles) versus temperature. The average hydrodynamic diameters reported were obtained as the first moment of the size distribution by number. f) Extinction spectrum of Ag-Ag₂S dimers dispersed in distilled water. In the inset, an optical image of Ag-Ag₂S dimer dispersion in water is shown. g) Results of the 3-(4,5-dimethylthiazol-2-yl)-2,5-diphenyltetrazolium bromide (MTT) assay used to evaluate the cytotoxicity of Ag-Ag₂S dimers in HeLa cells after 2 and 24 h of incubation at nanoparticle concentration ranging from 5 to 100 µg mL⁻¹. Ctrl = control (no nanoparticles).

Ag⁺ ions are added to this solution, no reduction to elemental Ag is observed. However, upon adjusting the pH to 9.0–9.5 with NaOH_{aq} 0.5 M, the addition of Ag⁺ is immediately followed by a darkening of the reaction mixture, due to the rapid nucleation and growth of Ag nanoparticles (Figure S1b, Supporting Information). It is reasonable to assume that this pH increase elevates the redox potential of the Ag⁺→Ag⁰ couple, hence favoring the reduction process due to more negative free energy. This reaction is like the classical Turkevich method for gold nanoparticles^[22] (and its modification by Lee-Mesiel for silver^[23]),

wherein sodium citrate is used simultaneously as a reducing and capping agent that controls the nucleation and growth of metal nanoparticles. Despite its long history, the citrate-mediated method still has some unsolved questions, which stem from the wealth of molecular species (e.g., radicals and oxidation products) formed during the nanoparticle nucleation and growth.^[24,25] This complexity is exacerbated in our method by the presence of several molecular species at different concentrations.^[26,27] Therefore, a thorough description of the reaction steps involved in the silver reduction process was not

attempted and it is realistically unachievable. Most importantly for our purposes, in the proposed method, introduction of Na_2S after the formation of Ag nanoparticles and readjustment of the pH to 9.0–9.5 led to the growth of Ag– Ag_2S dimers (Figure 2a).

The formation mechanism of these dimers is credibly the result of two simultaneous processes: heterogeneous nucleation of Ag_2S on preformed Ag nanoparticles and partial conversion of Ag to Ag_2S .^[28] As inferred from transmission electron microscope (TEM) observations, the final product of this reaction is an ensemble of dimeric nanoparticles with a variable Ag/ Ag_2S ratio and an ellipsoidal morphology, where the minor and major axes are 16 ± 3 and 19 ± 3 nm, respectively (Figure 2b). This architecture is typical of several reported “ Ag_2S ” nanoparticles—which are de facto Ag– Ag_2S dimers, and follows from the low reduction potential of Ag^+ ions along with the use of ligands exhibiting reducing capabilities (here, e.g., chlorogenic, ferulic, and *n*-coumaric acid).^[29] In our synthesis, we chose a pH value of 9.0–9.5 for two reasons: 1) to deprotonate the largest fraction of molecules in the coffee extract, as, for instance, some chlorogenic acids have pK_a constants well above 7^[30]; and 2) to avoid the precipitation of silver hydroxide and/or oxide, which occurs already at slightly higher alkaline pH values in pure water.^[31] Deprotonation of the molecules is necessary to increase their coordinating capabilities and thus their effectiveness in controlling the nanoparticle growth. In the optimized synthesis method, 3.0 mL of a 30 mg mL^{−1} coffee extract solution was used, for a total of ≈ 90 mg of dry extract. Lower amounts of coffee extract did not lead to monodispersed nanoparticles (Figure S3, Supporting Information). Likewise, a higher reaction temperature yielded a polydisperse sample (Figure S4, Supporting Information), while prolonging the reaction time had no noticeable effect on the reaction product (Figure S5, Supporting Information). Details regarding the exploration of the reaction parameters are reported in Supporting Information. It should be noted that the total amount of material obtained from the synthesis and calculated via gravimetry was 11 ± 2 mg. At first glance, this value agrees with at a first glance, agrees with the quantity of precursors, that is, 10.4 mg (0.1 mM) of Ag^+ and 1.5 mg (0.05 mM) of S^{2-} . However, the weight of the final product obtained via gravimetry includes molecules from the coffee extract attached to the nanoparticle surface. Indeed, from total X-ray fluorescence (TXRF) measurements, 7.6 ± 0.3 and 0.60 ± 0.03 mg of Ag^+ and S^{2-} were found, respectively, for a yield of $(69 \pm 3)\%$. This value accounts for material loss during the purification steps (i.e., centrifugation and filtration). The presence of molecules amounting up to $\approx 25\%$ of the weight of the sample is in line with previous reports.^[32]

It is worth mentioning at this point that, aside from Ag– Ag_2S dimers, we succeeded also in preparing small Ag_2S nanoparticles. An in-depth discussion around these nanoparticles is provided in the Supporting Information (Figure 1 and 6–8).

Returning our attention to the dimeric Ag– Ag_2S species, the presence of both Ag and Ag_2S in the sample was confirmed by X-ray powder diffraction (XRPD) measurements (Figure 2c). The diffractogram of the sample featured reflections characteristic of both materials. In addition, from quantitative TXRF measurements carried out on Ag– Ag_2S dimers, an Ag^+ -to- S^{2-} ratio of 3.74 was obtained. This is in stark contrast with the TXRF results

for Ag_2S nanoparticles (Figure S1d, Supporting Information), which returned a ratio of 2.16, much closer to the theoretical value of 2. Admittedly, in the case of dimers, the contribution to the silver signal might come from pure Ag nanoparticles present individually in the dispersion and whose presence, albeit not apparent in TEM images, cannot be completely ruled out.

The obtained dimers retain on their surface the molecules present in the coffee extract, as highlighted by the comparison between the Fourier-transform infrared (FTIR) spectra of the nanoparticles and the dried coffee extract (Figure 2d). The broad signal arising from O–H vibrations of residual water molecules and phenolic groups is observed between 4000 and 3000 cm^{−1}. The C–H symmetric and asymmetric stretching can be found to be around 2950 cm^{−1}, whereas a wealth of vibrations ascribed to the carbonyl moiety (C=O) appears between 1800 and 1680 cm^{−1}.^[33] The signals below 1600 cm^{−1} originate from vibrations from different groups, such as C–H scissoring (1450 cm^{−1}), C–N stretching (1250 cm^{−1}), and C–O stretching (1150 cm^{−1}). All these groups are found in roasted coffee extract and are part of complex carbohydrates (e.g., arabinogalactans and galactomannans).^[34] It should be noted that the main differences between the spectrum of the extract and of the dimers are observed in the 1800–1600 cm^{−1} range, where C=O stretching and other caffeine-related vibrations fall. These signals are suppressed in the dimer spectrum, which resembles closely in the 1900–500 cm^{−1} range the one of arabinogalactans (see, for instance, Figure 2 in the study by Capek et al.^[34]). This observation indicates that the surface chemistry of Ag– Ag_2S dimers is dominated by water-soluble carbohydrates found in the coffee extract. As confirmed by ζ -potential and dynamic light scattering (DLS) measurements, these molecules impart a net negative charge to the surface of the particles (Figure S9, Supporting Information), which ultimately translates to colloidal stability and lack of aggregation both in distilled water and in phosphate saline buffer (PBS 1x) between 15 and 55 °C (Figure 2e). This colloidal stability was maintained for at least 48 h in PBS 1x and in a 10% aqueous solution of fetal bovine serum (FBS) without noticeable effect on the hydrodynamic size of the nanoparticles (Figure S10, Supporting Information). It is reasonable to think that some of the molecules attached on the dimer surface may also impart steric colloidal stabilization aside from charge stabilization. From an optical standpoint, the Ag– Ag_2S dimers efficiently absorb the electromagnetic radiation in the visible and NIR-I range (Figure 2f). This strong, extended absorption featured by the Ag– Ag_2S dimers arises from the synergy between the plasmonic and semiconductor moieties (vide infra). In addition, no PL was displayed from these species, as opposed to Ag_2S nanoparticles, which featured weak NIR emission (Figure S11, Supporting Information). The weakness of the emission of Ag_2S nanoparticles results from the selected synthesis method, which is conducted in water using low-synthesis temperature. Indeed, oxygen, hydroxyl groups, and water molecules could be introduced in the particle volume and act as luminescence quenching centers.^[35] Moreover, the hydroxyl- and carboxyl-rich molecules present in the coffee extract that remain attached to the dimers' surface contribute to the quenching of the emission due to their high-energy vibrations.^[36] The fast formation of the nanoparticles upon addition of the sulfur source, likely yielding a defective crystal structure, is also to be taken into account to

explain the low-emission efficiency. In the case of Ag–Ag₂S, this quenching is exacerbated by the metal moiety, as it can act as an acceptor in electron transfer phenomena from the semiconductor.^[37] This pivotal role played by Ag was also confirmed with further experiments (see next section). Finally, we tested the *in vitro* toxicity of the Ag–Ag₂S dimers toward HeLa cells. The lack of appreciable short- and long-term cytotoxicity (Figure 2g), along with their colloidal stability, make these Ag–Ag₂S dimers amenable to use in biological environments.

Overall, the proposed reaction adheres to at least five out of ten principles of green chemistry: 1) less hazardous chemical synthesis; 2) safer solvents and auxiliaries; 3) design for energy efficiency; 4) use of renewable feedstocks; and 5) safer chemistry for accident prevention. Adherence to these principles is guaranteed by the use of natural aqueous coffee extract and the conduction of all the synthesis steps (coffee extraction and nanoparticle synthesis) at room temperature. A point should be made regarding Na₂S, which is known for being corrosive and toxic. However, for water-based synthesis, it represents a safer choice in terms of storage and handling than H₂S. Unfortunately, the much safer and inert elemental sulfur is instead practically insoluble in water.

One might question the general applicability of the developed synthesis method, as we investigated the system using a specific brand of coffee. To test the robustness of the approach, we prepared coffee extracts of three additional brands and attempted the synthesis of Ag–Ag₂S dimers. We followed the same recipe developed for the coffee extract so far discussed, keeping for all brands the same final amount (90 mg) of coffee extract in the reaction mixture and the other parameters unaltered. In all cases, we obtained dimeric structures that closely resembled the ones obtained with the thoroughly investigated coffee extract so far discussed (Figure S12, Supporting Information). Although a larger variability of the size was observed for the three newly synthesized samples, this is still a stunning result, considering that different coffee extracts might feature sizably different chemical compositions. Hence, the results shown in Figure S12 (Supporting Information), along with the remarkably similar spectra recorded for the samples synthesized using different coffee brands (Figure S13, Supporting Information), are proof of the general applicability of the developed method and that only minor adjustments are likely required when changing the coffee extract.

2.2. Switching on the Luminescence of Ag–Ag₂S Dimers

Intrigued by the utter lack of emission displayed by the Ag–Ag₂S dimers, we then tested the possibility of making them photoluminescent upon controlled oxidation (Figure 3).

This approach has recently been proposed by Zhang et al. on Ag–Ag₂S nanocomposites, observing that the luminescence increased as a result of a decreased amount of metallic Ag in the system.^[10] The authors claimed that the fluorescence quenching mechanism was the result of electron transfer between Ag and Ag₂S moieties. Electron transfer mechanisms at the interface between plasmonic structures and semiconductors are well documented in fields such as photocatalysis and photovoltaics.^[38,39] It is thus reasonable to ascribe this switching on of the

luminescence to a marked reduction or total removal of the electronic communication between the moieties originally comprising the Ag–Ag₂S dimer upon H₂O₂-mediated oxidation.

In our case too, by simply introducing controlled amounts of H₂O₂ in an aqueous dimer dispersion and stirring at room temperature for several days, we started observing the emergence of an emission peak centered around 1250 nm under 784 nm excitation (Figure 3a). The rate at which this increase was observed was proportional to the concentration of H₂O₂. However, at the highest tested concentration (1.5 M), the fast PL increase within 2 days was followed by an equally steep emission quenching over the following days. This quenching is likely to be attributed to the appearance of defects at the Ag₂S surface following prolonged exposure to the oxidizer and continuous stirring at room temperature. A slower but larger increase was instead observed for H₂O₂ concentrations of 0.1 and 0.5 M. Although more time-consuming, a slower oxidation allows to reach more intense PL, while also granting a wider time window to stop the process when the maximal intensity is achieved.

The oxidation was conducted at higher temperatures too (Figure S14, Supporting Information), observing a similar trend to the one obtained varying the H₂O₂ concentration: Higher temperatures speed up the process but also induce an earlier quenching and a lower achievable overall PL intensity. To understand this process, TEM images were taken of the dimers before and after subjecting them to oxidation (Figure 3b). Comparison of these images highlighted, on average, the reduction of the dimension of silver moiety, with some particles bearing a “hole” where the metallic particle was located. This effect was expected from the visual comparison of the suspension before and after exposure to H₂O₂ (Figure 3c). Such visual cue was mirrored by the change in the extinction spectrum (Figure 3d), which acquired a profile more closely resembling the one of Ag₂S nanoparticles (Figure S7, Supporting Information). This experimental observation was further corroborated by the results of theoretical simulations, which predict an analogous spectral change upon removal of the silver moiety.

In particular, computational results show that the presence of Ag inclusions close to the surface of an Ag₂S sphere introduces a broad contribution to the overall extinction of the system (Figure 4). Although most notable at wavelengths above 500 nm, this Ag-related contribution spans most of the spectrum of the Ag–Ag₂S dimers. Reinforcing our interpretation of the optical data in Figure 2f and 3d, the inclusion of an embedded Ag nanoparticle in Ag₂S leads to a significantly different spectrum compared with the one of an isolated metallic nanoparticle. Removal of the silver moiety results in a reduction of the extinction in the visible range, which parallels the color change witnessed upon H₂O₂ treatment (Figure 3c). Discrepancies between the simulated spectra of individual nanoparticles and extinction spectra of Ag–Ag₂S dimers recorded experimentally are attributed to polydispersion in terms of Ag–Ag₂S geometries and Ag sizes. We should mention that, although the TEM data suggest that the Ag crystals are fully embedded in Ag₂S, we have also explored configurations with Ag protruding to different degrees (Figure S15, Supporting Information), which could also contribute to the overall spectrum of the nanoparticle ensemble. Finally, as expected from the fact that the nanoparticle size was much smaller than the wavelength of the impinging photons, our

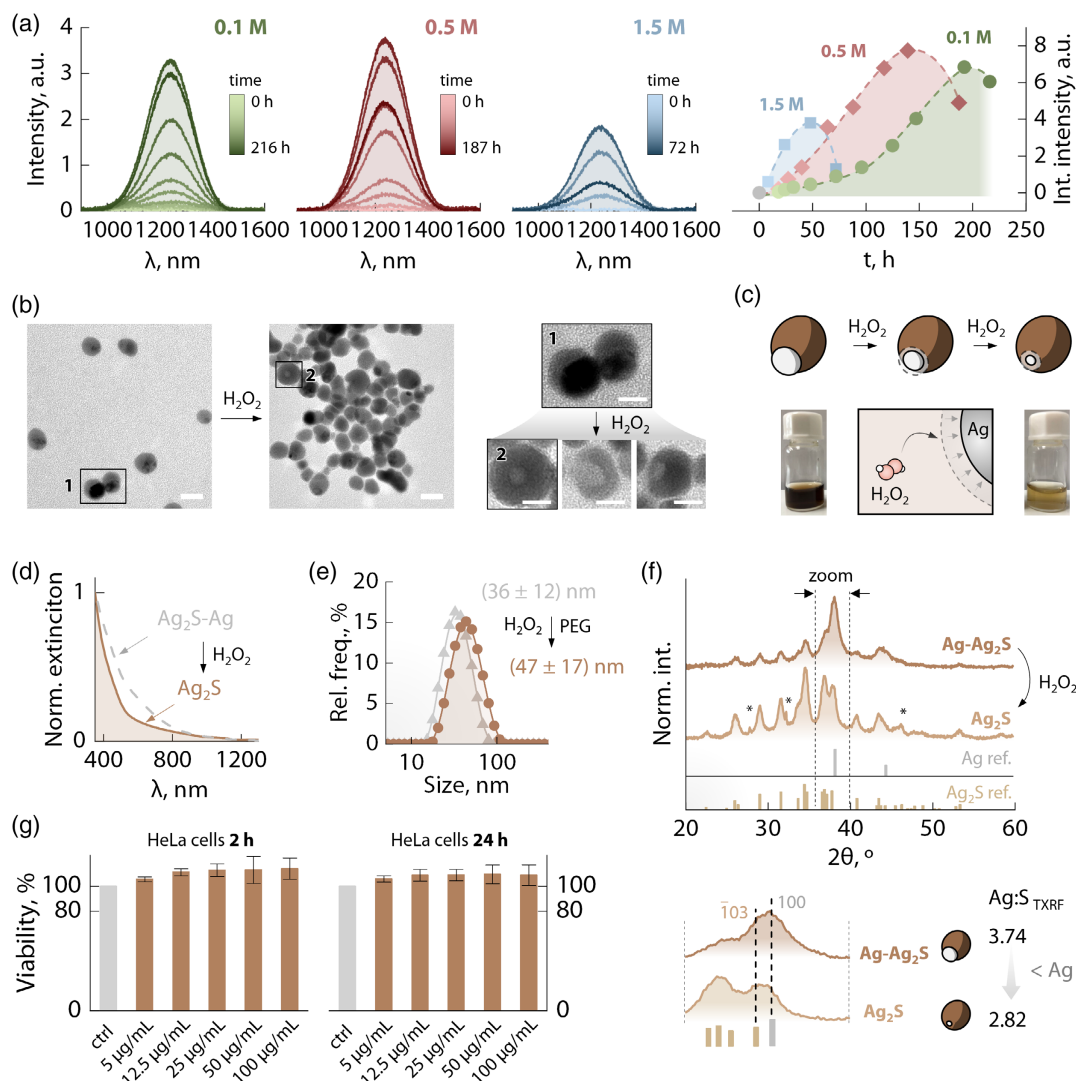


Figure 3. Characterization of oxidized Ag–Ag₂S dimers. a) Temporal evolution of Ag–Ag₂S PL following treatment with different concentrations of H₂O₂: 0.1 M (green), 0.5 M (red), and 1.5 M (blue). b) TEM images before and after H₂O₂ treatment (at [H₂O₂] = 0.5 M and after 147 h). After oxidation, the number of particles with large Ag moiety is reduced, and some once dimers even show complete removal of the metallic part, as evidenced by the comparison of particle close-ups. c) Sketch of the H₂O₂-mediated oxidation process, along with optical pictures taken before (left vial) and after (right vial) oxidation. d) Change of the extinction spectrum of the Ag–Ag₂S dimers (gray dashed line) upon oxidation to Ag₂S (brown solid line). e) Increase in the hydrodynamic size of the nanoparticles after oxidation and surface modification with PEG-SH. f) Diffraction patterns of Ag–Ag₂S and Ag₂S nanoparticles (i.e., before and after oxidation) compared with reference diffraction patterns of Ag (PDF #00-004-0783, gray bars) and Ag₂S (PDF #00-014-0072, golden bars). Weak and sharp reflections ascribed to AgCl are indicated with asterisks. A zoom-in of the 36–40° region is presented at the bottom, along with the Ag-to-S ratio obtained from TXRF analysis. g) Results of the MTT assay used to evaluate the cytotoxicity of Ag₂S nanoparticles in HeLa cells after 2 and 24 h of incubation at nanoparticle concentration ranging from 5 to 100 μg mL^{−1}. Ctrl = control (no nanoparticles). Here, Ag₂S is used as a shorthand for indicating the final product of oxidation, although excess silver is still present in the nanoparticles after partial oxidation.

computational models confirmed that the light scattering is negligible compared with the absorption (Figure S16, Supporting Information).

Importantly, the H₂O₂ treatment affects the colloidal stability of Ag–Ag₂S dimers, likely due to oxidation of the molecules passivating the surface of the dimers and their detachment during silver removal. For this reason, the surface of the oxidized nanoparticles was modified with PEG-SH (2 kDa), ultimately leading to increased colloidal stability and a hydrodynamic size increase to 47 ± 17 nm (Figure 3e). This colloidal stability was maintained

for at least 48 h in PBS 1x and in a 10% solution of FBS in water without noticeable effect on the hydrodynamic size of the nanoparticles (Figure S17, Supporting Information). Despite loss of colloidal stability, this controlled oxidation does not lead to substantial changes in the overall morphology of the particles (Figure S18, Supporting Information). Further confirmation of the removal of elemental silver was obtained from the XRPD pattern of the sample after treatment with H₂O₂, wherein the reflections ascribed to cubic Ag⁰ decreased sizably in intensity (Figure 3f). A zoom-in of the diffraction patterns in the 36–40° range

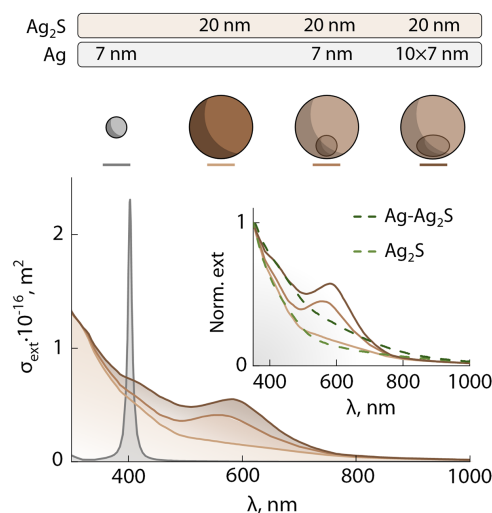


Figure 4. Computational extinction profiles of four systems that are representative of the observed pure and hybrid moieties. The diagrams above the plot are sketches showcasing the geometries of the systems. In the last two of them, the Ag₂S sphere is semitransparent to show the embedded Ag geometries. In the inset, the extinction spectra, normalized at 350 nm, are reported for the simulated Ag–Ag₂S geometries (solid brown lines) along with the measured spectra of Ag–Ag₂S dimers before (dark green dashed line) and after (light green dashed line) oxidation.

more clearly allows to visualize this change, with the peak centered at around 38° shifting toward smaller angles due to an increased contribution of the (103) Ag₂S reflection. Moreover, TXRF analysis indicated that the Ag-to-S ratio changed from the initial 3.74 of the dimers to ≈ 2.82 after oxidation, further corroborating the partial removal of silver. Weak, sharp reflections ascribed to AgCl were observed after oxidation (indicated with asterisks in Figure 3f). Their appearance indicates the formation of AgCl impurities from the reaction of solubilized Ag⁺ and traces of Cl[−] in deionized water.^[40] Finally, the cytotoxic effect of the nanoparticles obtained after H₂O₂ treatment was investigated on HeLa cells (Figure 3g). The results of these experiments showed no significant decrease in cell viability after 4 and 24 h of incubation at the tested concentrations.

2.3. Thermometric Capabilities

To further characterize the optical properties of the oxidized nanoparticles, we investigated the thermal dependence of their absolute intensity (Figure 5a) and average lifetime (Figure 5b). A reversible quenching of the emission intensity (also accompanied by a bathochromic shift; Figure S19, Supporting Information) and a shortening of the lifetime was observed. The calibration curves obtained from the analysis of the emission spectra and decay curves recorded at different temperatures showed a similar trend, which translated to a relative sensitivity (S_R) at room temperature of $\approx 3\% \cdot ^\circ\text{C}$ in both cases (Figure S20, Supporting Information). This value is remarkably similar to the sensitivities reported for other Ag₂S-based nanoparticles used in luminescence thermometry.^[41] Comparing the measured PL lifetime of approx. 120 ns at 25 °C with a dataset of PL quantum yield

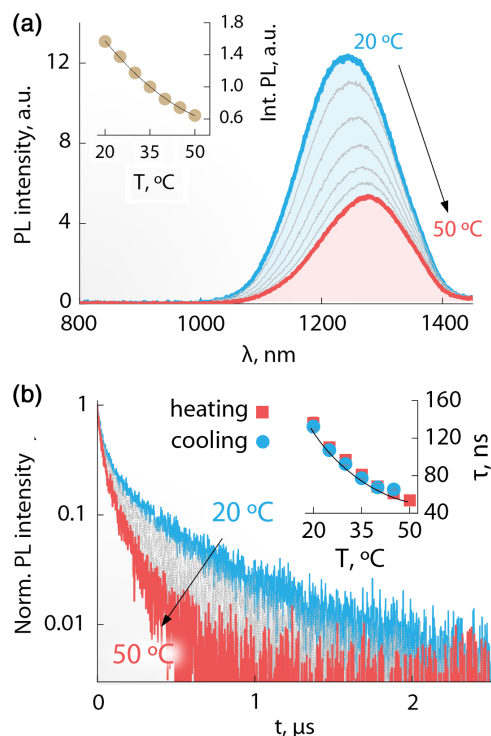


Figure 5. Luminescence thermometry with Ag₂S nanoparticles obtained from H₂O₂-mediated oxidation of Ag–Ag₂S dimers. a) Emission spectra recorded under 784 nm excitation in the 20–50 °C range and corresponding calibration curve obtained from averaging the results of three heating cycles. The integrated values for each cycle were normalized to the integrated intensity at 35 °C, close to the normal temperature of the body (37 °C). b) Decay curves recorded monitoring the emission at 1250 nm under 800 nm excitation in the 20–50 °C range along with the corresponding calibration curve. The experimental points of the calibration curve were obtained from a heating–cooling cycle.

(PLQY) versus lifetime obtained from the literature, a PLQY of $\approx 0.1\%$ was estimated for the oxidized dimers at that temperature (Figure S21, Supporting Information). This value is on par with typical values of commercial Ag₂S nanocrystals.^[42]

Overall, the results of the optical characterization of the oxidized Ag–Ag₂S dimers highlight the good fluorescence properties of the developed material and their amenability to use in FI.

2.4. Application of the Nanoparticles for Imaging

To confirm the prowess and versatility of Ag–Ag₂S dimers as imaging contrast agents, they were used for PAI and FI, respectively, before and after H₂O₂ treatment (Figure 6a). The strong absorption, minimal photon scattering, and lack of emission featured by as-synthesized Ag–Ag₂S dimers make them ideal PAI contrast agents. This combination of optical properties endows them with photon-to-heat conversion capabilities. The local temperature variations induced by the absorption of the probing photons from the contrast agent translate to the generation of elastic waves (Figure 6b), which are detected from the PAI detector.

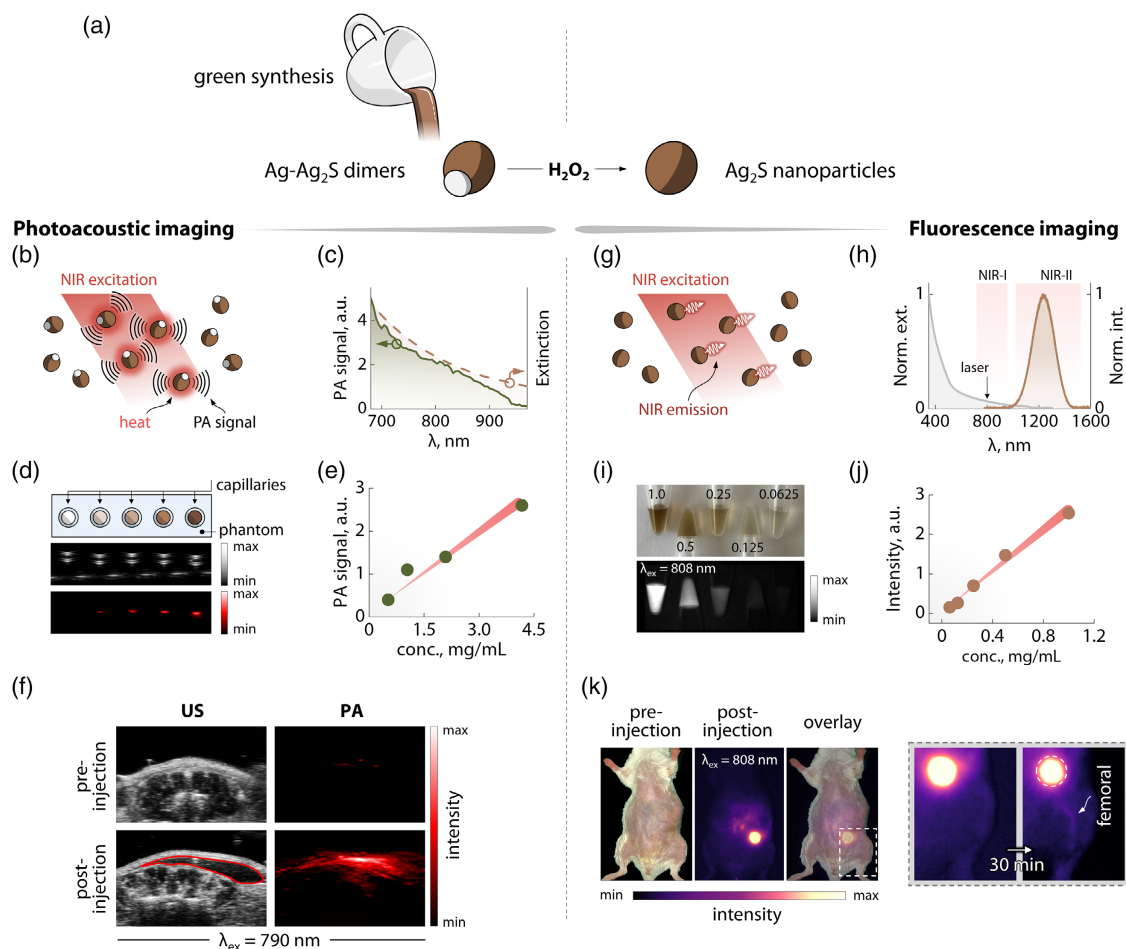


Figure 6. Evaluation of the performance of Ag–Ag₂S dimers before and after oxidation (i.e., H₂O₂ treatment) as PAI and FI contrast agents. a) Sketch of the steps described in this study for the preparation and subsequent oxidation of Ag–Ag₂S dimers. b) Sketch of the working principle of Ag–Ag₂S as PAI contrast agent. c) Photoacoustic (PA) spectrum (solid green line) and extinction spectrum (brown dashed line) of Ag–Ag₂S dimers. d) Scheme (top), ultrasound (US, center), and PA (bottom) images of capillaries filled with different concentrations (0.5, 1, 2, 4 mg mL^{−1}) of PBS 1× dispersions of Ag–Ag₂S recorded under broadband (690–970 nm) excitation. e) PAI signal versus Ag–Ag₂S concentration obtained from the analysis of the image in (d). f) In vivo US and PAI images of a mouse's abdomen before (top) and after (bottom) subcutaneous injection of 50 µL of 4 mg mL^{−1} dispersion of Ag–Ag₂S dimers. g) Sketch of the working principle of Ag₂S as FI contrast agents. h) Absorption (gray line) and emission (brown line) spectra of Ag₂S. First and second biological windows (NIR-I and NIR-II) are also indicated. i) Optical (top) and NIR (bottom) images of 1.5 mL centrifuge tubes filled with different concentrations (1, 0.5, 0.25, 0.125, 0.0625 mg mL^{−1}) of Ag₂S dispersions in PBS 1×. j) NIR signal versus Ag₂S concentration obtained from the analysis of the image in (i). k) In vivo NIR FI images obtained after intraperitoneal injection of 50 µL of a 1 mg mL^{−1} dispersion of Ag₂S nanoparticles. On the left, a zoom-in of the left hind limb immediately after and 30 min after injection is shown. In the rightmost figure, femoral vessels that became visible after diffusion of the contrast agents in the vasculature are indicated with an arrow and the original extension of the NIR signal at the injection site is delineated with a white dashed circle.

We therefore initially tested the Ag–Ag₂S dimers in vitro. The PAI excitation spectrum was collected in the 670–970 nm range, observing a remarkably similar trend of the PAI signal and the absorption spectrum of the dimers (Figure 6c). We then collected a calibration curve, using a setup composed of plastic channels submerged in Agar-based hydrogel, which acts as an optical phantom (Figure 6d and S22, Supporting Information). The channels were filled with decreasing concentration of Ag–Ag₂S dimers in PBS 1× (4, 2, 1, 0.5 mg mL^{−1}). The PAI signal recorded under broadband excitation in the 670–970 nm range showed a linear trend with the concentration (Figure 6e). Subsequently,

we moved to the in vivo level, injecting subcutaneously 50 µL of 4 mg mL^{−1} dispersion of Ag–Ag₂S dimers.

A comparison of the photoacoustic images recorded pre- and postinjection using an excitation wavelength of 790 nm clearly highlights an increased signal at the injection site (area delineated in red in Figure 6f).

Finally, oxidized Ag–Ag₂S dimers (simply Ag₂S henceforth) subjected to PEGylation were used in FI. Their absorption of NIR photons in the first and emission in the second biological windows, respectively (NIR-I and NIR-II), fulfils the pivotal requirements for a FI contrast agent (Figure 6g,h). Similar to

the process followed for PAI, we initially measured a calibration curve in vitro, filling different 1.5 mL tubes with dispersions of Ag₂S in PBS 1× at decreasing concentrations (1, 0.5, 0.25, 0.125, 0.0625 mg mL⁻¹; Figure 6i) and measured the average NIR emission intensity under 808 nm excitation. A linear correlation between the NIR intensity and the Ag₂S concentration was retrieved (Figure 6j). After having ascertained the properties of the nanoparticles in vitro, 50 µL of 1 mg mL⁻¹ Ag₂S dispersion were administered to a mouse via intraperitoneal injection (Figure 6k). Immediately after injecting the contrast agents, a strong NIR signal was recorded at the administration site under 808 nm excitation. After 30 min, the nanoparticles started diffusing, as confirmed by a reduction of the NIR signal extension at the injection site, along with the appearance in the NIR image of the femoral vessels. This observation further confirms the robustness of the herein-presented FI contrast agents for in vivo applications, as they retained their luminescence in a biological environment throughout the imaging experiments. Furthermore, the possibility of easily replacing the ligands on the surface of Ag₂S using thiol-bearing moieties (as testified by the straightforwardness of the PEGylation protocol used) paves the way for decoration of the nanoparticles' surface with targeting molecules. One strategy might entail the use of bifunctional carboxy-PEG-thiols, which would result in the presence of exposed –COOH groups, thus allowing coupling of, for example, tumor-targeting peptides via carbodiimide-mediated crosslinking (i.e., EDC–NHS coupling).

3. Conclusion

We have developed a green synthesis method for the preparation of Ag₂S-based nanoparticles whose optical properties can be readily tuned to act as contrast agents for PAI or NIR FI. Coffee extract was used as the source of reducing and coordinating molecules capable of directing the growth of the nanoparticles at room temperature. Investigation of the reaction parameters allowed identifying the addition order of the reactants, pH, and coffee extract concentration as key aspects of the synthesis protocol. Among the obtainable nanoparticles, Ag–Ag₂S dimers feature strong light absorption extending in the NIR and negligible emission, making them amenable for use in PAI imaging. However, their NIR luminescence can be switched on via controlled oxidation of Ag moieties, thus making them suitable contrast agents for FI. Theoretical calculations allowed confirming the role played by Ag in determining the light extinction properties of Ag–Ag₂S and corroborated the interpretation of the spectral changes observed upon treating the dimers with H₂O₂. Indeed, this induced switching on of the fluorescence is of interest also for developing activable probes capable of signaling in vivo the generation of H₂O₂, which is known to occur during the growth and expansion of certain solid tumors.

Overall, the results presented herein demonstrate that green approaches can be developed for preparing nanoparticles with tangible potential in real-life applications. The developed method, in hand with the presented theoretical model, also provides further insight into the complex chemistry and physics of NIR-active Ag₂S-based nanomaterials. We wish this investigation will spur further study on simple, environmentally friendly

chemical processes for the preparation of nanoparticles made of an ever-broader fan of materials.

Supporting Information

Supporting Information is available from the Wiley Online Library or from the author.

Acknowledgements

R.M. acknowledges the support of the European Commission through the European Union's Horizon 2020 research and innovation program under the Marie Skłodowska-Curie Grant agreement N° 797945 (LANTERNS). L.V.B. acknowledges the support of the Xunta de Galicia (Centro singular de investigación de Galicia accreditation 2019-2022), the European Union (European Regional Development Fund, ERDF), and the National Natural Science Foundation of China (project no. 12050410252). A.B. acknowledges funding from Comunidad de Madrid through TALENTO grant ref. 2019-T1/IND-14014. This work was supported by the Spanish Ministry of Economy and Competitiveness under projects MAT2016-75362-C3-1-R, MAT2017-83111R, MAT2017-85617-R, and PID2019-106211RB-I00, by the Instituto de Salud Carlos III (PI16/00812), by the Comunidad Autónoma de Madrid (B2017/BMD-3867 RENIM-CM), and cofinanced by the European structural and investment fund. Additional funding was provided by the European Union's Horizon 2020 FET Open programme (Grant agreement no. 801305, NanoTBTech), the Fundación para la Investigación Biomédica del Hospital Universitario Ramón y Cajal project IMP18_38 (2018/0265), and also COST action CA17140. D.M.-G. acknowledges "Fundación para la investigación biomédica del Hospital Ramón y Cajal" (FIBioHRYC) and the European Commission Horizon 2020 project NanoTBTech (grant number: 801305) for postdoctoral funding. J.Y. acknowledges the support from the China Scholarship Council (CSC File No. 201704910867).

Conflict of Interest

The authors declare no conflict of interest.

Data Availability Statement

Data available on request from the authors.

Keywords

Ag₂S, coffee, green syntheses, near infrared, photoacoustic

Received: August 25, 2021

Revised: September 18, 2021

Published online: November 25, 2021

- [1] <https://www.un.org/development/desa/disabilities/envision2030-goal12.html>.
- [2] H. Agarwal, S. Venkat Kumar, S. Rajeshkumar, *Resour.-Eff. Technol.* **2017**, *3*, 406, <https://www.un.org/development/desa/disabilities/envision2030-goal12.html>.
- [3] S. Iravani, *Green Chem.* **2011**, *13*, 2638.
- [4] M. Behravan, A. Hossein Panahi, A. Naghizadeh, M. Ziaee, R. Mahdavi, A. Mirzapour, *Int. J. Biol. Macromol.* **2019**, *124*, 148.

- [5] P. P. Dutta, M. Bordoloi, K. Gogoi, S. Roy, B. Narzary, D. R. Bhattacharyya, P. K. Mohapatra, B. Mazumder, *Biomed. Pharmacother.* **2017**, 91, 567.
- [6] N. Gonzalez-Ballesteros, S. Prado-Lopez, J. B. Rodriguez-Gonzalez, M. Lastra, M. C. Rodriguez-Arguelles, *Colloids Surf. B Biointerfaces* **2017**, 153, 190.
- [7] Y. Shen, J. Lifante, E. Ximendes, H. D. A. Santos, D. Ruiz, B. H. Juarez, I. Zabala Gutierrez, V. Torres Vera, J. Rubio Retama, E. Martin Rodriguez, D. H. Ortgies, D. Jaque, A. Benayas, B. Del Rosal, *Nanoscale* **2019**, 11, 19251.
- [8] C. Lu, G. Chen, B. Yu, H. Cong, *Adv. Eng. Mater.* **2018**, 20, 1700940.
- [9] T. Yang, Y. Tang, L. Liu, X. Lv, Q. Wang, H. Ke, Y. Deng, H. Yang, X. Yang, G. Liu, Y. Zhao, H. Chen, *ACS Nano* **2017**, 11, 1848.
- [10] X. Zhang, W. Wang, L. Su, X. Ge, J. Ye, C. Zhao, Y. He, H. Yang, J. Song, H. Duan, *Nano Lett.* **2021**, 21, 2625.
- [11] E. Ximendes, R. Marin, Y. Shen, D. Ruiz, D. Gomez-Cerezo, P. Rodriguez-Sevilla, J. Lifante, P. X. Viveros-Mendez, F. Gamez, D. Garcia-Soriano, G. Salas, C. Zalbidea, A. Espinosa, A. Benayas, N. Garcia-Carrillo, L. Cusso, M. Desco, F. J. Teran, B. H. Juarez, D. Jaque, *Adv. Mater.* **2021**, 33, e2100077.
- [12] Y. Du, B. Xu, T. Fu, M. Cai, F. Li, Y. Zhang, Q. Wang, *J. Am. Chem. Soc.* **2010**, 132, 1470.
- [13] A. Ortega-Rodriguez, Y. Shen, I. Zabala Gutierrez, H. D. A. Santos, V. Torres Vera, E. Ximendes, G. Villaverde, J. Lifante, C. Gerke, N. Fernandez, O. G. Calderon, S. Melle, J. Marques-Hueso, D. Mendez-Gonzalez, M. Laurenti, C. M. S. Jones, J. M. Lopez-Romero, R. Contreras-Caceres, D. Jaque, J. Rubio-Retama, *ACS Appl. Mater. Interfaces* **2020**, 12, 12500.
- [14] B. Yuan, T. K. Egner, V. Venditti, L. Cademartiri, *Nat. Commun.* **2018**, 9, 4078.
- [15] P. Jiang, C. N. Zhu, Z. L. Zhang, Z. Q. Tian, D. W. Pang, *Biomaterials* **2012**, 33, 5130.
- [16] C. Zhang, S. Zhang, L. Yu, Z. Zhang, P. Zhang, Z. Wu, *Mater. Lett.* **2012**, 85, 77.
- [17] S. I. Sadovnikov, Y. V. Kuznetsova, A. A. Rempel, *Nano-Struct. Nano-Objects* **2016**, 7, 81.
- [18] D. Ayodhya, G. Veerabhadram, *J. Photochem. Photobiol. B* **2016**, 157, 57.
- [19] V. G. Debabov, T. A. Voelikova, A. S. Shebanova, K. V. Shaitan, L. K. Emel'yanova, L. M. Novikova, M. P. Kirpichnikov, *Nanotechnol. Russ.* **2013**, 8, 269.
- [20] G. V. de Melo Pereira, D. P. de Carvalho Neto, A. I. Magalhaes Junior, F. G. do Prado, M. G. B. Pagnoncelli, S. G. Karp, C. R. Soccol, *Adv. Food Nutr. Res.* **2020**, 91, 65.
- [21] N. Z. Rao, M. Fuller, *Sci. Rep.* **2018**, 8, 16030.
- [22] J. Turkevich, P. C. Stevenson, J. Hillier, *Discuss. Faraday Soc.* **1951**, 11, 55.
- [23] P. C. Lee, D. Meisel, *J. Phys. Chem.* **1982**, 86, 3391.
- [24] M. Wuthschick, A. Birnbaum, S. Witte, M. Sztucki, U. Vainio, N. Pinna, K. Rademann, F. Emmerling, R. Kraehnert, J. Polte, *ACS Nano* **2015**, 9, 7052.
- [25] J. Kimling, M. Maier, B. Okenve, V. Kotaidis, H. Ballot, A. Plech, *J. Phys. Chem. B* **2006**, 110, 15700.
- [26] N. Wang, L. T. Lim, *J. Agric. Food Chem.* **2012**, 60, 5446.
- [27] G. R. Lopes, C. P. Passos, C. Rodrigues, J. A. Teixeira, M. A. Coimbra, *Eur. Food Res. Technol.* **2019**, 245, 2133.
- [28] D. Wang, T. Xie, Q. Peng, Y. Li, *J. Am. Chem. Soc.* **2008**, 130, 4016.
- [29] J. Huang, T. Lei, M. Siron, Y. Zhang, S. Yu, F. Seeler, A. Dehestani, L. N. Quan, K. Schierle-Arndt, P. Yang, *Nano Lett.* **2020**, 20, 3734.
- [30] Y. Maegawa, K. Sugino, H. Sakurai, *Free Radical Res.* **2007**, 41, 110.
- [31] H. L. Johnston, F. Cuta, A. B. Garrett, *J. Am. Chem. Soc.* **1933**, 55, 2311.
- [32] R. Marin, A. Skripka, L. V. Besteiro, A. Benayas, Z. Wang, A. O. Govorov, P. Canton, F. Vetrone, *Small* **2018**, 14, e1803282.
- [33] D. J. Lyman, R. Benck, S. Dell, S. Merle, J. Murray-Wijelath, *J. Agric. Food Chem.* **2003**, 51, 3268.
- [34] P. Capek, E. Paulovicova, M. Matulova, D. Mislovicova, L. Navarini, F. Suggi-Liverani, *Carbohydr. Polym.* **2014**, 103, 418.
- [35] S. W. Buckner, R. L. Konold, P. A. Jelliss, *Chem. Phys. Lett.* **2004**, 394, 400.
- [36] A. Skripka, A. Benayas, C. D. S. Brites, I. R. Martin, L. D. Carlos, F. Vetrone, *Nano Lett.* **2020**, 20, 7648.
- [37] W. Park, D. Lu, S. Ahn, *Chem. Soc. Rev.* **2015**, 44, 2940.
- [38] S. K. Cushing, J. Li, J. Bright, B. T. Yost, P. Zheng, A. D. Bristow, N. Wu, *J. Phys. Chem. C* **2015**, 119, 16239.
- [39] A. Furube, S. Hashimoto, *NPG Asia Mater.* **2017**, 9, e454.
- [40] M. Y. Kamentsev, S. N. Mamedova, L. N. Moskvina, N. M. Yakimova, *J. Anal. Chem.* **2015**, 70, 193.
- [41] D. Ruiz, B. del Rosal, M. Acebrón, C. Palencia, C. Sun, J. Cabanillas-González, M. López-Haro, A. B. Hungría, D. Jaque, B. H. Juarez, *Adv. Funct. Mater.* **2017**, 27, 1604629.
- [42] H. D. A. Santos, I. Zabala Gutierrez, Y. Shen, J. Lifante, E. Ximendes, M. Laurenti, D. Mendez-Gonzalez, S. Melle, O. G. Calderon, E. Lopez Cabarcos, N. Fernandez, I. Chaves-Coira, D. Lucena-Agell, L. Monge, M. D. Mackenzie, J. Marques-Hueso, C. M. S. Jones, C. Jacinto, B. Del Rosal, A. K. Kar, J. Rubio-Retama, D. Jaque, *Nat. Commun.* **2020**, 11, 2933.